Optical Code Division Multiple Access Network Transmission With *M*-ary Chip Symbols

Aminata A. Garba and Jan Bajcsy

***Abstract*—This paper uses *M*-ary chip symbols to increase the spectral efficiency of optical code division multiple access (OCDMA) even though, when compared to its binary counterpart, *M*-ary OCDMA can have significantly increased multi-user interference (MUI). The presented numerical channel capacity results show that appropriate *non-uniform* *M*-ary signaling allows the reduction of MUI and the achievement of improved OCDMA spectral efficiency. Using insights from the OCDMA capacity results, we design a coded *M*-ary OCDMA transmission scheme that can achieve very high spectral efficiencies. The proposed time/wavelength OCDMA scheme relies on intensity modulation, appropriate non-uniform signaling, *M*-ary trellis-coded modulation and error-correcting codes. The corresponding receiver is based on direct detection of optical signals, soft-decision single-user demodulation and error-control decoding. The presented simulation results illustrate that the designed OCDMA scheme can support hundreds of active users at the target bit error rate of 10^{-9} and is robust to impairments encountered in optical transmission (shot noise, thermal noise). The achieved spectral efficiency of up to 1.34 bits per OCDMA chip is significantly better than the best binary OCDMA result reported in the literature.**

***Index Terms*—*M*-ary optical code division multiple access (OCDMA) transmission; Non-uniform signaling; Single-user soft-decision demodulation and iterative decoding; Spectrally efficient asynchronous OCDMA.**

I. Introduction

Optical code division multiple access (OCDMA) has been widely explored as a technology for military, government and commercial optical networks, e.g., in [1–15]. OCDMA can offer secure and flexible network transmission based on the broadcast and select approach, direct sequence spreading and/or time/frequency hopping. Since users in OCDMA networks are non-orthogonal and asynchronous, severe multi-user interference (MUI) has been a key factor limiting the performance of OCDMA transmission in both theoretical and experimental studies. Although utilizing *M*-ary OCDMA instead of the traditional binary OCDMA would seem to be a natural approach to increase the achieved spectral efficiency, *M*-ary signaling by non-orthogonal users usually leads to worse MUI than binary signaling. Consequently, binary OCDMA has been mostly studied in the literature so far.

This paper presents results illustrating that *M*-ary OCDMA can be used in such a way that it significantly outperforms binary OCDMA. The comparison is done in terms of achieved spectral efficiency and ability to support many active OCDMA users concurrently. We present relevant channel capacity results and simulated bit error rate (BER) performance of a coded *M*-ary OCDMA system to show that the use of *M*-ary chip symbols can increase data rates in OCDMA networks when compared to binary OCDMA systems. As in most prior literature, we focus on OCDMA with single-user demodulation and decoding (SUD) due to practical implementation complexity constraints and signal processing speed requirements.

The structure of this paper is as follows. Section II includes channel and noise models that describe MUI, the considered optical channel imperfections and channel noise. Consequently, Section III presents a channel capacity analysis for the considered *M*-ary optical CDMA transmission. In Section IV, we present the design of a coded OCDMA transmission scheme that is based on non-uniform *M*-ary channel input signaling, convolutional error-correcting codes (ECC), the designed trellis-coded modulation and time/wavelength hopping. The corresponding receiver, described in the same section, uses soft-decision (single-user) demodulation and iterative (turbo) processing. Section V presents the simulation results for the described *M*-ary OCDMA transmission corrupted by MUI, Poisson shot noise and additive white Gaussian noise (AWGN) thermal noise. Finally, Section VI concludes the paper.

II. Channel Models

A. Overall Assumptions

We consider *M*-ary OCDMA network transmission with SUD at the receiver. *K* independent users (i.e., users who do not cooperate) send frame-asynchronous and chip-synchronous information data simultaneously over a fiber-optic channel, e.g., using a star coupler. (The chip-synchronous assumption represents the worst case of chip-level interference.) During the modulation, transmission and demodulation processes, the optical signals are assumed to add up incoherently without beatings and optical intensity direct detection is used at the receiver.

Manuscript received October 27, 2010; revised January 28, 2011; accepted February 9, 2011; published April 28, 2011 (Doc. ID 137259).

The authors are with the Electrical and Computer Engineering Department, McGill University, 3480 University St., Montréal, Québec H3A 2A7, Canada (e-mail: aminata.amadougarba@mail.mcgill.ca).

Digital Object Identifier 10.1364/JOCN.3.000435

 © 2011 Optical Society of America

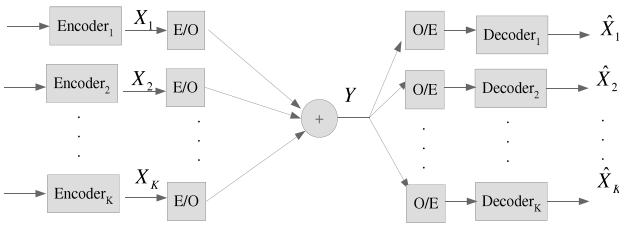

Fig. 1. Schematic block diagram of OCDMA network transmission with SUD at the receiver.

Under the above assumptions, we first describe a K-user coded M-ary optical CDMA transmission at the chip level with appropriate discrete-time memoryless channel models, as illustrated in Fig. 1. The input of the multi-access channel is the random variable X_1 representing the symbol sent by user 1, who is considered without any loss of generality. Channel input X_1 is consequently corrupted by interfering chip symbols $X_2, X_3, \ldots, X_K$ sent by other users and other sources of channel noise. We assume that for all users, M-ary chip symbols $x_i = 0,1,2,\ldots,M-1$ are sent with probabilities $p_0, p_1, \ldots, p_{M-1}$.

We consider three types of OCDMA transmission:

1) idealized interference-only channel, when the transmitted symbol X_1 is corrupted only by MUI $(X_2 + \cdots + X_K)$;
2) low power OCDMA transmission when symbols are corrupted by both the MUI and Poisson shot noise from the users' transmitters;
3) OCDMA channel with MUI and thermal noise from receiver electronics.

The following three subsections describe these channels in further detail.

B. Interference-Only OCDMA Channel Model

For the interference-only channel, the output of the OCDMA channel is given by the random variable Y:

$$Y = X_1 + X_2 + \cdots + X_K, \tag{1}$$

which can take values of $0,1,\ldots,K(M-1)$. Y represents the sum of the chip symbols sent by all K users of the network at a given time instant. The entries of the resulting chip-level channel matrix $P_{Y|X_1}$ are the conditional probabilities of the output symbol given the input symbol and can be described for all $y \in \{0,1,2,\ldots,K(M-1)\}$ and $x_1 \in \{0,1,2,\ldots,M-1\}$ by

$$P_{Y|X_1}(Y = y|X_1 = x_1) = \sum_{\substack{(x_2,x_3,\ldots,x_K)\in\{0,1,2,\ldots,M-1\}^{K-1} \\ \text{s.t.} \\ x_2+x_3+\cdots+x_K=(y-x_1)}} p_{x_2} p_{x_3} \cdots p_{x_K}, \tag{2}$$

where $p_x = P(X_i = x)$.

C. OCDMA Channel With Optical Shot Noise

We consider the case when the dominant noise affecting OCDMA transmission is due to optical shot noise at the optical transmitters, e.g., in the case of low power/low loss transmission. We will assume that μ is the average number of photons used by each user to distinguish consecutive M-ary levels in chip transmission. Given that user i wants to transmit data symbol $x_i \in \{0,1,2,\ldots,(M-1)\}$, the number of photons sent by his optical transmitter is conditionally Poisson distributed with mean $x_i\mu$. Consequently, when users $1,2,\ldots,K$ send symbols $x_1, x_2, \ldots, x_K$, channel output Y, which represents the total number of photons received at the receiver counting detector, is also conditionally Poisson distributed with a mean $\mu(x_1 + x_2 + \cdots + x_K) = \mu s$, i.e.,

$$P_{Y|X_1,\ldots,X_K}\left(Y = y|X_1 = x_1,\ldots,X_K = x_K\right) = \frac{e^{-\mu s}(\mu s)^y}{y!},$$

for all integers $y = 0,1,2,\ldots$. In addition, the conditional probability mass function fully describing this single-user decoded channel is given by

$$P_{Y|X_1}(Y = y|X_1 = x_1) = \sum_{s=0}^{K(M-1)} \frac{e^{-\mu s}(\mu s)^y}{y!} \times \sum_{\substack{(x_2,x_3,\ldots,x_K)\in\{0,1,2,\ldots,M-1\}^{K-1} \\ \text{s.t.} \\ x_2+x_3+\cdots+x_K=(s-x_1)}} p_{x_2} p_{x_3} \cdots p_{x_K}, \tag{3}$$

for all $x_1 = 0,1,\ldots,M-1$ and $y = 0,1,2,\ldots$.

D. OCDMA Channel Model With Thermal Noise

In the case where the thermal noise from the receiver electronics is the dominant external noise, the output of the OCDMA channel is given by

$$Y = X_1 + X_2 + \cdots + X_K + v. \tag{4}$$

In this case, channel input X_1 is corrupted by MUI $\left(X_2 + \cdots + X_K\right)$ as well as the Gaussian-distributed thermal noise v from the receiver electronics that is assumed to have zero mean and variance of σ^2. Consequently, the conditional probability density describing this channel is given by

$$f_{Y|X_1}(y|x_1) = \frac{1}{\sqrt{2\pi}\sigma} \sum_{x_2=0}^{M-1} \sum_{x_3=0}^{M-1} \cdots \sum_{x_K=0}^{M-1} \left(e^{\frac{-1}{2\sigma^2}\left(y - \sum_{i=1}^{K} x_i\right)^2} \prod_{i=2}^{K} p_{x_i} \right), \tag{5}$$

for all real numbers y. In this case, we will define a normalized channel signal to noise ratio (SNR) per chip as $SNR = 1/\sigma^2$, so that it is independent of the channel input probabilities.

III. Channel Capacity Results and Insights

A. Channel Capacity for OCDMA Transmission

We will use the *symmetric sum capacity* as an upper limit on the aggregate *data throughput* achievable by the considered K symmetric OCDMA users during network transmission. This capacity can be used as a benchmark when maximizing the *spectral efficiency* of a designed OCDMA system. When SUD is used, the sum capacity can be theoretically calculated by maximizing the mutual information between the channel input chip symbol X_1 and the channel output Y over all channel input probability mass functions P_{X_1}:

$$C = K \sup_{P_{X_1}} I(X_1;Y). \tag{6}$$

The units of this capacity/spectral efficiency limit are normalized to bits per OCDMA chip. Note that for a specific channel input probability mass function (PMF) P_{X_1}, we also define the *achievable throughput* as $K \times I(X_1;Y)$ evaluated for P_{X_1}. The achievable throughput gives a spectral efficiency limit when the OCDMA transmitters use this particular channel input PMF.

For the case of the interference-only OCDMA channel from Subsection II.B, we have numerically determined the exact sum capacity in [14] and it can be achieved using an appropriate non-uniform channel input PMF. To simplify the design of modulators/demodulators in Section IV, we will use throughout this paper the following near-optimal channel input PMF:

$$p_0 = 1 - \frac{1}{K} \quad \text{and} \quad p_1 = p_2 = \cdots = p_{M-1} = \frac{1}{K(M-1)}, \tag{7}$$

which is close to the capacity-achieving optimal input PMF from [14]. Consequently, using the channel input probability mass function from Eq. (7), we calculate the achievable throughput for

1) the interference-only OCDMA transmission described in Subsection II.B,
2) the shot noise dominated optical CDMA transmission discussed in Subsection II.C, and
3) the OCDMA channel with AWGN-distributed thermal noise from Subsection II.D.

B. Throughout Results for Interference-Only OCDMA

It can be seen in Fig. 2 that, when all M-ary inputs are used with equal probability and the number of users K increases, the OCDMA spectral efficiency limit converges to 0.72 bits per OCDMA chip, even when the number of modulation levels M increases from $M = 2$ to $M = 4, 8, 16$. However, it is interesting to observe from Fig. 2 that the OCDMA network throughput can be significantly enhanced by increasing the number of modulation levels and using non-uniform channel input PMFs given by Eq. (7).

Indeed, although increasing the number of modulation levels is expected to increase the amount of MUI, the use of the non-uniform input PMF from Eq. (7) keeps the MUI reduced. Figure 3 illustrates the reduced MUI obtained with non-uniform channel input PMF and compares it to the much larger amount of MUI resulting from uniform channel input signaling. This reduction of the MUI through non-uniform signaling allows increase of the theoretically achievable spectral efficiency to almost 2 bits per chip for $M = 16$.

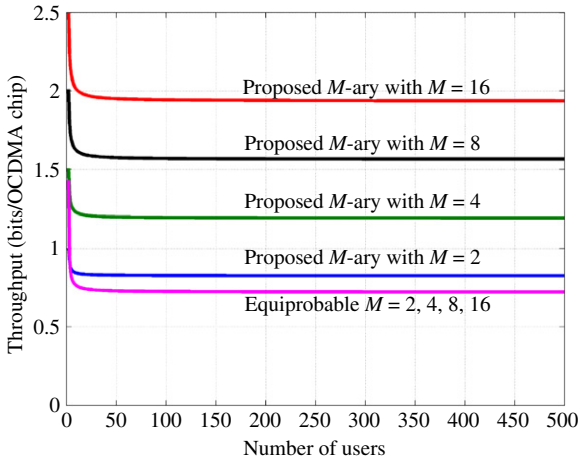

Fig. 2. (Color online) Theoretically achievable rates for an interference-only OCDMA network transmission with SUD.

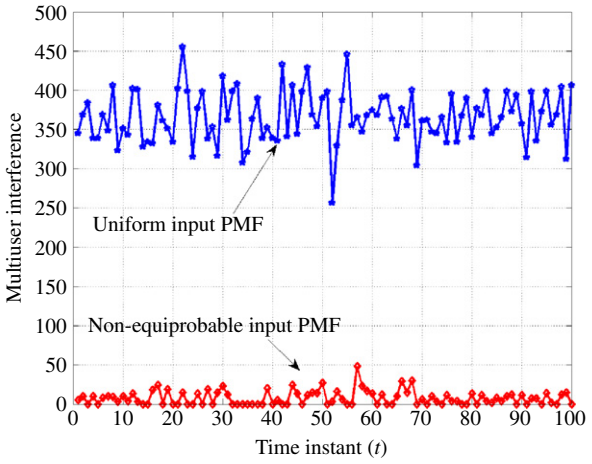

Fig. 3. (Color online) Comparison of the amount of OCDMA MUI in the cases of uniform and non-uniform channel input PMF from Eq. (7). The MUI is shown for different time instants t for $K = 50$ active OCDMA users and $M = 16$ modulation levels.

Moreover, as also illustrated in Fig. 2, the achievable aggregate throughput is steady for increasing number of active users and does not drop to zero. This is explained by the fact that the considered near-optimal input PMF from Eq. (7) depends on the number of active users and the probability of the MUI exceeding a given (often small number) is very low. Therefore, even if the total number of active users increases, the amount of MUI does not increase much.

Another key observation is that the MUI, when using the non-uniform channel input PMF from Eq. (7), turns out to be

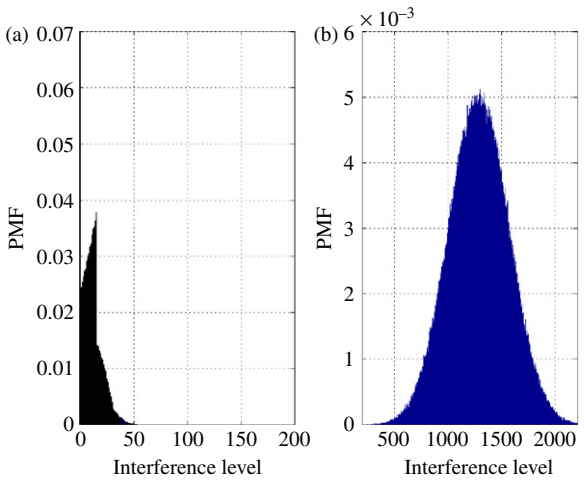

Fig. 4. (Color online) Histogram of MUI for 16-ary ($M = 16$) OCDMA transmission with $K = 300$ users. (a) *Non-Gaussian* MUI for non-uniform signaling $p_0 = 0.9967; p_1 = \cdots = p_{15} = 0.00022$. (b) *Gaussian* interference with uniform PMF: $p_0 = p_1 = \cdots = p_{15} = 1/16$.

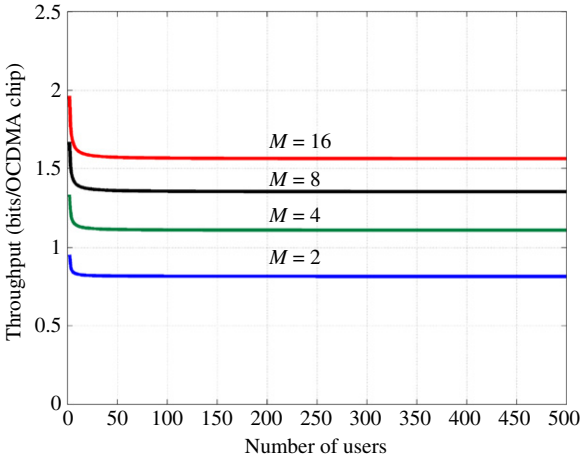

Fig. 5. (Color online) Achievable throughput as a function of the number of users for selected M-ary OCDMA transmission with SUD at the receiver when the average number of transmitted photons is $\mu = 20$ per M-ary level.

strongly reduced and *non-Gaussian*, as illustrated in Fig. 4 for an OCDMA network transmission, when 16-ary chip symbols are used with the proposed probabilities from Eq. (7). On the other hand, many traditional approaches to OCDMA network transmission with single-user decoding assume uniform chip symbols, and the MUI converges in distribution to a Gaussian random variable due to the central limit theorem. In such a case, the transmitted data end up being severely corrupted by the MUI, as also shown for illustration purposes in Fig. 4.

Consequently, since non-uniform channel input signaling leads to a reduced MUI and larger achievable transmission rates, we will consider OCDMA transmission with non-uniform channel input PMF for the rest of this paper.

C. Achievable Rates for OCDMA With Shot Noise

This section considers capacity limits on OCDMA transmission affected by shot noise. Achievable rates for optical CDMA network transmission corrupted by Poisson-distributed shot noise are evaluated using the near-optimal channel input PMF from Eq. (7). Figures 5, 6 and 7 contain the main capacity results that were obtained numerically and will be discussed in the following paragraphs.

In Fig. 5, the achievable transmission rates are shown for selected cases of M-ary modulation ($M = 2, 4, 8, 16$) when $\mu = 20$ photons per M-ary modulation level are transmitted and near-optimum channel input PMF from Eq. (7) is utilized. OCDMA network throughput of about 1.6 bits per chip is theoretically achievable in this case for $M = 16$ and a large number of active users. Although there is a capacity decrease due to the shot noise (compared to the capacity for $M = 16$ and interference only as illustrated in Fig. 2), a plateau is reached for $M = 2, 4, 8, 16$ and increasing number of users. So even though the amount of shot noise increases with the number of users K, the OCDMA throughput does not drop asymptotically.

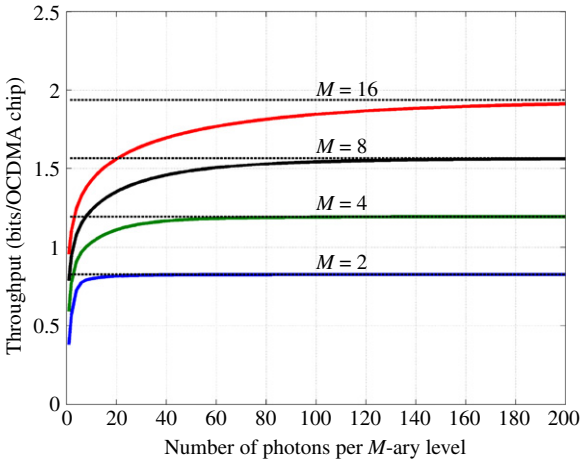

Fig. 6. (Color online) Achievable throughput as a function of μ, the number of transmitted photons per M-ary level, when the number of users is $K = 500$ for selected M-ary OCDMA transmission with SUD at the receiver. (The horizontal dashed lines represent the limiting cases without shot noise for the considered M-ary OCDMA systems.)

Figure 6 illustrates the dependence of the throughput on the average number of photons per OCDMA level (denoted μ), for a fixed number of active OCDMA users ($K = 500$) and binary, quaternary, 8-ary and 16-ary OCDMA symbols. One can observe in this figure that for small values of μ the achievable throughput is lower than the throughput achievable in the interference-only case, due to the effects of shot noise. Nonetheless, the performance of the interference-only OCDMA transmission can eventually be reached by increasing the average number of photons per M-ary level. However, although using $\mu = 20$ photons per binary level may be sufficient to (almost) achieve the interference-only throughput with binary OCDMA modulation, more than 80 photons per OCDMA level are required for 16-ary modulation to achieve a similar objective. Hence, as the number of modulation levels increases,

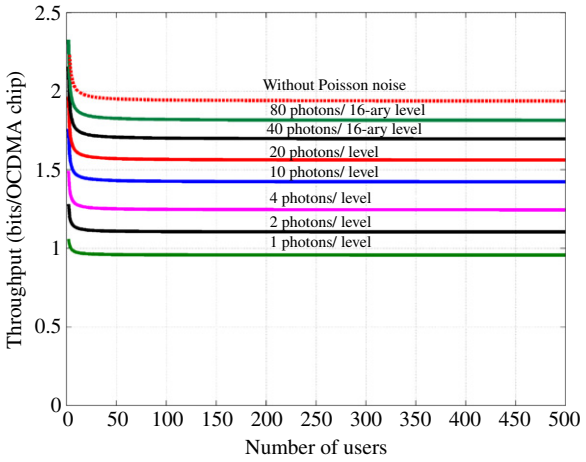

Fig. 7. (Color online) Achievable throughput limits on 16-ary OCDMA transmission with SUD at the receiver for different numbers of users K and numbers of photons per OCDMA level μ.

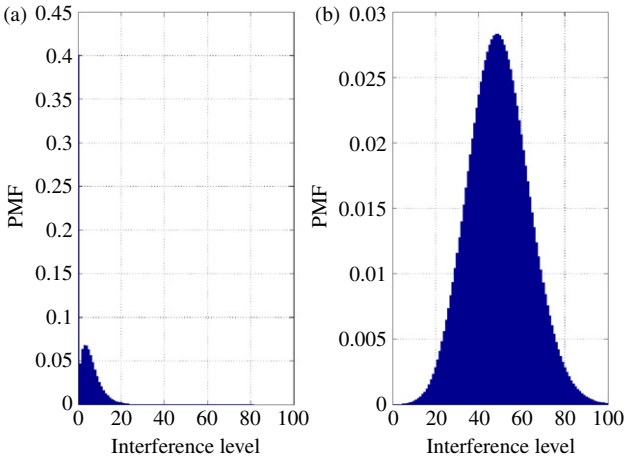

Fig. 8. (Color online) Histogram of MUI and shot noise for 16-ary ($M = 16$) OCDMA transmission with $K = 50$ users and $\mu = 1$. (a) *Non-Gaussian* MUI for near-optimal non-uniform channel input PMF: $p_0 = 0.98; p_1 = \cdots = p_{15} = 0.013$. (b) *Gaussian* interference with uniform PMF: $p_0 = p_1 = \cdots = p_{15} = 1/16$.

the average number of photons μ should be increased accordingly to allow better separation of user symbols from the shot noise effects. Finally, since the achievable throughput increases in Fig. 6 with increasing number of modulation levels M, one can conclude that OCDMA throughput gains due to non-uniform M-ary signaling are robust to shot noise effects.

Figure 7 illustrates, in the specific case of $M = 16$ modulation levels, the throughput limits for different numbers of active users and increasing average number of photons per OCDMA level. Not surprisingly, the aggregate throughput can be enhanced by increasing the average number of photons used to separate different M-ary levels. However, even with average separation of one photon per 16-ary OCDMA level, the achievable throughput does not drop to zero, but reaches a plateau of about half the capacity without shot noise. This result is rather surprising, as only about a half of the interference-only capacity would have been lost due to the shot noise if a super-low power transmitter had been used. Finally, it can be observed that with about 80 photons per 16-ary OCDMA level, it is possible to approach the limiting capacity of the interference-only transmission.

Finally, Figs. 8 and 9 show the combined MUI and shot noise affecting OCDMA transmission in the cases of near-optimal non-uniform chip signaling (a) and uniform chip signaling (b). One can observe the reduced and non-Gaussian nature of the channel impairments affecting the transmitted symbols in the case of near-optimal non-uniform signaling from Eq. (7).

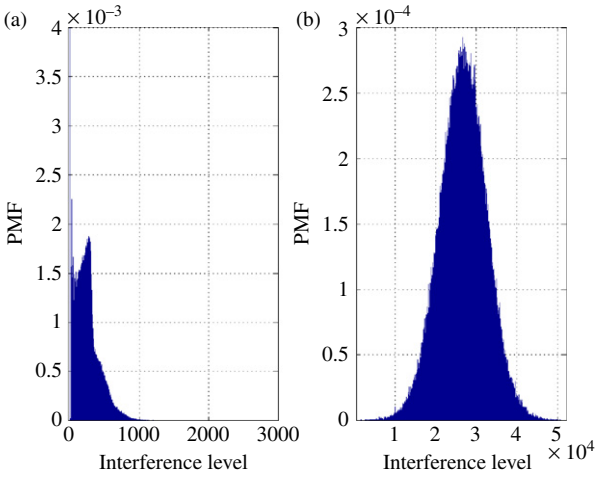

Fig. 9. (Color online) Histogram of MUI and shot noise for 16-ary ($M = 16$) CDMA transmission with $K = 300$ users and $\mu = 20$. (a) *Non-Gaussian* MUI with non-uniform, near-optimal channel input PMF: $p_0 = 0.9967; p_1 = \cdots = p_{15} = 0.00022$. (b) *Gaussian* interference with uniform PMF: $p_0 = p_1 = \cdots = p_{15} = 1/16$.

D. Throughout Results for OCDMA With Gaussian Noise

This subsection explores the throughput limits for selected M-ary OCDMA transmission with SUD in the presence of thermal AWGN noise due to the receiver electronics. We use the near-optimum non-uniform signaling from Eq. (7) and numerically evaluate the channel throughput limits for different values of M and signal to noise ratios.

First, we observe how the OCDMA throughput limit changes at a fixed chip-level SNR. Figure 10 shows that for $SNR = 20$ dB, the achievable spectral efficiency is close to the interference-only case considered in Fig. 2 in Subsection III.B. This shows the robustness of the proposed OCDMA scheme to a practical amount of AWGN noise.

Figure 11 presents additional results that illustrate how the throughput limit for M-ary OCDMA transmission increases almost linearly with increasing SNR until it reaches a saturation level. This saturation plateau occurs at around 15 dB chip-level SNR for $M = 2, 4, 8, 16$ modulation levels and is equal to the throughput limit of the same M-ary system in the absence of noise (interference-only case). Consequently, as

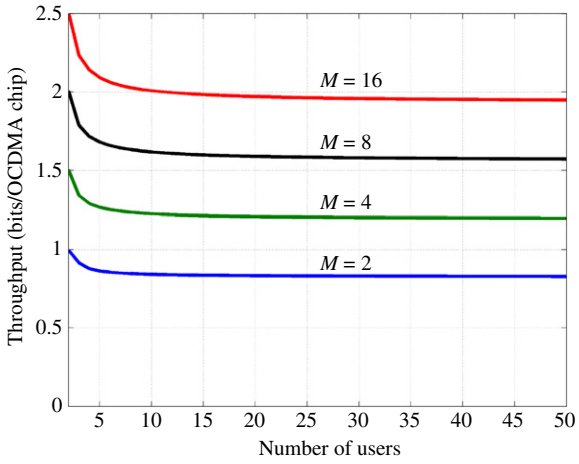

Fig. 10. (Color online) Achievable throughput against number of users for the selected M-ary OCDMA transmission with SUD at the receiver at 20 dB chip SNR.

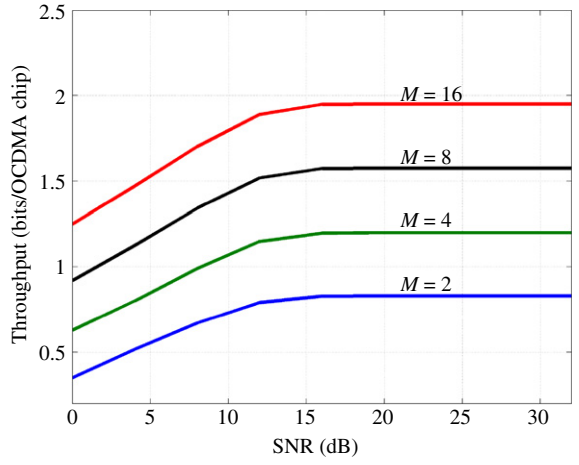

Fig. 11. (Color online) Achievable throughput as a function of chip SNR for the selected 50-user M-ary CDMA transmission with SUD at the receiver.

the SNR increases, the spectral efficiency can be significantly improved with M-ary modulation using the non-uniform channel input PMF from Eq. (7), when compared to both binary and uniform M-ary OCDMA transmission.

IV. Proposed OCDMA Transmission Scheme

Our aim is to design a scheme for OCDMA network transmission and reception that exploits the capacity gains of OCDMA with non-uniform M-ary chips from Section III. We extend our recently proposed wavelength–time OCDMA-spreading approach [15] from binary to the case of M-ary modulated symbols and also incorporate an additional M-ary trellis-coded modulator (TCM) as well as an iterative receiver that uses turbo-demodulation. In addition, we also describe three single-user OCDMA demodulators that allow soft-decision demodulation of a signal corrupted by MUI and shot (or thermal) noise.

A. Proposed Transmission Scheme

Figure 12 shows the overall schematic block diagram of the considered optical CDMA network transmission scheme with K users transmitting data simultaneously, frame asynchronously and independently of each other. Each user's data packet is first encoded using a Reed–Solomon code, then interleaved and encoded by a convolutional code. Consequently, the encoded data are modulated using a TCM which maps the encoded binary packet into an M-ary data stream composed of equiprobable symbols $0,1,2,\ldots,M-1$.

Each TCM encoded packet is consequently sent through a user-specific OCDMA modulator that uses wavelengths $\lambda = 1,2,3,\ldots,\Lambda$ and time slots $t = 1,2,3,\ldots$ for data transmission. As shown in detail in Fig. 13, the modulator first arranges error-control coded bits of a given user into consecutive two-dimensional arrays of size Λ by T. Consequently, it pads each array with Z columns, all containing zero symbols, where

$$Z = T \times \frac{K(M-1)-M}{M}. \tag{8}$$

These deterministic zero symbols, which we will call *zero-padded* symbols, are inserted into the stream of modulated M-ary chip symbols in order to achieve near capacity-achieving channel input probability from Eq. (7). Afterward, a user-specific channel time-interleaver pseudo-randomly permutes the columns of each 2-dimensional data array to distribute data and padded symbols evenly in the transmitted packets. Finally, the user's data are optically modulated by the E/O module shown in Fig. 12. The optical intensity signal $x_i(t,\lambda)$, sent at time t and wavelength λ, corresponds to the appropriate entry of the 2-dimensional data arrays sent by user i.

As a result of this OCDMA modulation approach, the channel use probability by each active user is

$$P_{ch} = \frac{M}{K(M-1)}. \tag{9}$$

Note that P_{ch} corresponds to the fraction of the time when a user sends error-control coded chip symbols directly over the channel, as opposed to sending the zero-padded symbols.

B. Proposed Receiver

As illustrated in Fig. 12, the proposed single-user receiver is composed of an appropriate optical to electrical signal converter (O/E), a soft-decision OCDMA demodulator and an iterative decoder that is followed by a Reed–Solomon decoder, all separated by appropriate interleaving/de-interleaving. The O/E module of the OCDMA receiver first performs intensity detection for each separate time–wavelength slot, thus generating electrical signals proportional to the received signal $y(t,\lambda)$ at each time instant t and for each wavelength slot λ. Consequently, at each time instant t for which the user sent a coded data symbol over the channel (i.e., not a padded

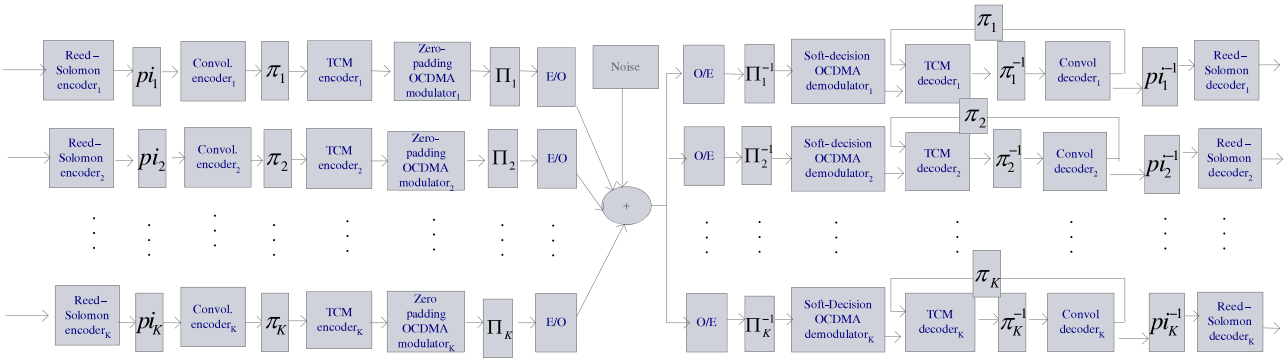

Fig. 12. (Color online) Schematic block diagram of the proposed OCDMA transmission scheme with SUD at the receiver. (Electro-optic and opto-electric signal conversion is performed by the E/O and O/E modules and data interleaving/de-interleaving is performed by modules denoted by $pi_i, \pi_i, \Pi_i, \pi_i^{-1}, \Pi_i^{-1}, pi_i^{-1}$).

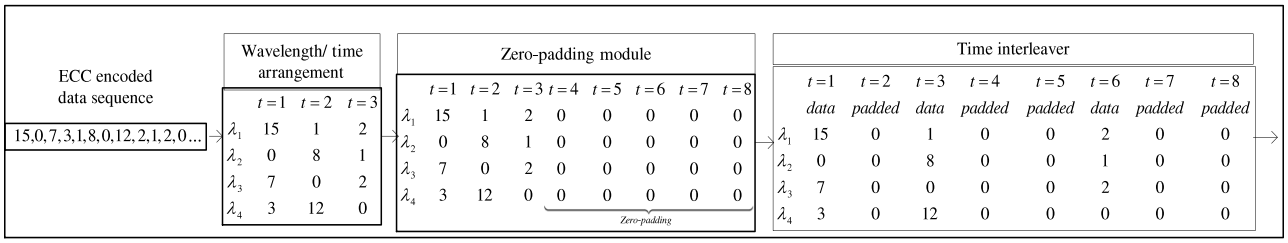

Fig. 13. Detailed operation of the proposed M-ary wavelength–time OCDMA modulator: twelve symbols that were error-control encoded and 16-ary TCM encoded are rearranged into a time/wavelength array with parameters $T = 3$ and $\Lambda = 4$, padded with $Z = 5$ all-zero columns and time-interleaved prior to being sent through the optical channel.

0 symbol), we use an appropriate chip-level soft-decision OCDMA demodulator defined in the next subsection. The demodulator generates *a posteriori* probability estimates about the M-ary TCM coded symbols of the desired user which are then fed into a soft-decision TCM decoder and an error-correcting convolutional decoder. The TCM and convolutional decoders are connected in an iterative decoding loop in which they exchange extrinsic information estimates about the error-control coded bits by applying the turbo-demodulation approach from [16]. After a prescribed number of iterations, the convolutional decoder passes its hard decisions to the Reed–Solomon decoder that estimates the message bits of the desired user.

C. Soft-Decision Demodulators

We describe the design of several M-ary OCDMA demodulators to be used in the architecture of Fig. 12 in the presence of various channel impairments. The OCDMA single-user demodulators use the appropriate channel model from Eq. (3) or Eq. (5) and the Bayes' rule to generate *a posteriori* probability estimates about the coded M-ary chip symbols of a given user.

These *a posteriori* probabilities about the coded bits of desired user 1 are given for the OCDMA channel with Poisson shot noise as

$$P_{X_1|Y}(x_1(t,\lambda)=m|y(t,\lambda)) = \alpha \sum_{j=0}^{K_t(M-1)} \frac{e^{-\mu j}(\mu j)^{y(t,\lambda)}}{y(t,\lambda)!} P_{j|m} \tag{10}$$

and for OCDMA transmission with AWGN thermal noise as

$$P_{X_1|Y}(x_1(t,\lambda)=m|y(t,\lambda)) = \alpha \sum_{j=0}^{(K_t-1)(M-1)} e^{\frac{-1}{2\sigma^2}(y(t,\lambda)-(m+j))^2} P_{j|m}. \tag{11}$$

Note that in the two previous equations, α denotes a normalization constant and K_t is the number of users transmitting data (not zero-padded symbols) at time t (Appendix A describes a way in which K_t can be determined in practice.) Finally, $P_{j|m}$ represents the conditional probability that the sum $X_1 + X_2 + \cdots + X_K$ is equal to j when the channel input $X_1 = m$, i.e., $P_{j|m} = Pr(X_1 + X_2 + \cdots + X_K = j | X_1 = m)$. This quantity can be evaluated for all $j = 0, 1, 2, \ldots, K(M-1)$ and $m = 0, 1, 2, \ldots, M-1$ as follows:

$$P_{j|m} = \sum_{\substack{(x_2,x_3,\ldots,x_K)\in\{0,1,2,\ldots,M-1\}^{K-1} \\ \text{s.t.} \\ x_2+x_3+\cdots+x_K=(y-x_1)}} p_{x_2} p_{x_3} \cdots p_{x_K}. \tag{12}$$

V. Simulation Results

This section presents BER performance results for the M-ary OCDMA transmission scheme from Fig. 12 in the presence of MUI and noise (shot or AWGN). The OCDMA target BER is 10^{-9} and the simulated results presented in this section show that the considered M-ary OCDMA architecture from Fig. 12 can achieve high spectral efficiencies of up to 1.34 bits per OCDMA chip.

A. System Parameters

We considered a 16-ary ($M = 16$) OCDMA network transmission system with SUD at the receiver. We employed a (255, 239) Reed–Solomon code over a Galois field (GF) (256) [17] followed by the rate 1/2 convolutional encoder with the generator polynomials of the constituent encoders being $g_1(D) = 1 \oplus D^3 \oplus D^4$ and $g_2(D) = 1 \oplus D \oplus D^3 \oplus D^4$.

Figure 14 shows the trellis diagram of a 16-ary non-recursive TCM encoder with 16 states and rate two that was designed using Ungerboeck's set-partitioning rules [18]. The two binary input symbols and the corresponding 16-ary output symbol are illustrated for the four transitions ending at each state.

The time/wavelength OCDMA modulators used $\Lambda = 62$ wavelengths for data transmission and channel access probability $P_{ch} = 0.0032$. The system also used a 63rd wavelength to determine K_t, the number of actively interfering users at each time instant t, and a 64th wavelength for other protocols, as discussed in Appendix A. User-specific pseudo-random channel interleavers are utilized to permute M-ary TCM symbols on the chip level. We also used pseudo-random interleavers of length 10,000 between the error-correcting encoder (Reed–Solomon and convolutional encoder) and the TCM encoder.

The soft-decision TCM and convolutional decoders, connected in an iterative decoding loop shown in Fig. 12, used the BCJR algorithm [19]. The Reed–Solomon decoder is applied after a prescribed number of decoding iterations to lower the end-to-end BER below the target value of 10^{-9}.

The achieved spectral efficiency at the target BER of 10^{-9} is determined for the proposed architecture in Fig. 12 as the aggregate rate of the coding and modulation schemes for all the K users of the network as follows:

$$\eta = \underbrace{K}_{\text{Number of users}} \times \underbrace{R_c}_{\text{ECC Code rate}} \times \underbrace{R_{\text{mod}}}_{\text{Rate of the OCDMA modulator}} \text{ bits/ OCDMA chip}, \tag{13}$$

where K is the total number of active OCDMA users that can be supported on the network at BER = 10^{-9}, R_c is the combined rate of the convolutional, TCM and Reed–Solomon codes (respectively R_{CC}, R_{TCM}, R_{RS}). Finally, R_{mod} is the rate of the zero-padding OCDMA modulator which can be calculated as $R_{\text{mod}} = P_{ch} \times \frac{62}{64}$, where P_{ch} is the probability of channel use defined in Eq. (9) defining the ratio of the number of actual data symbols over the number of combined data and zero-padded symbols. The number 62/64 above represents the ratio of the number of wavelengths used for actual data transmission over the total number of wavelengths (since two wavelengths have been dedicated to determine K_t and other network considerations).

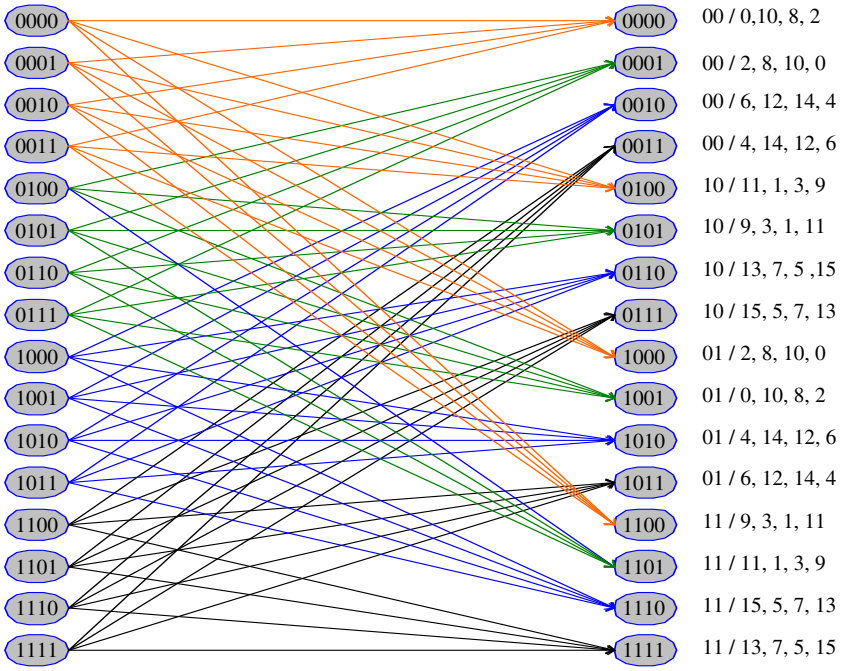

Fig. 14. (Color online) One stage of the designed trellis diagram for the rate two, 16-ary TCM encoder. (Note: all trellis edges entering a given state have the same input labels.)

Consequently, the spectral efficiency can be written as

$$\eta = K \times (R_{CC} \times R_{TCM} \times R_{RS}) \times \left(P_{ch} \times \frac{62}{64}\right) \text{ bits/OCDMA chip.} \quad (14)$$

B. BER Performance Results

We first considered an OCDMA transmission where the Poisson shot noise is the dominant noise. Initially, the considered number of photons per 16-ary modulation level is limited to $\mu = 20$ and Fig. 15 illustrates the obtained BER performance. It can be seen that up to $K = 298$ active users can be supported at the target BER $= 10^{-9}$ after seven iterations of the iterative decoder followed by Reed–Solomon decoding. This corresponds to an achieved spectral efficiency of

$$\eta = 298 \times \left(\frac{1}{2} \times 2 \times \frac{239}{255}\right) \times \frac{62}{64} \times P_{ch} = 0.86 \text{ bits/OCDMA chip.}$$

After increasing the average number of photons to $\mu = 40$ photons per 16-ary level, Fig. 16 presents the simulated BER performance results. The number of supported users on the OCDMA network is $K = 368$ active users, after 10 decoding iterations and Reed–Solomon decoding. This corresponds to an achieved spectral efficiency of

$$\eta = 368 \times \left(\frac{1}{2} \times 2 \times \frac{239}{255}\right) \times \frac{62}{64} \times P_{ch} = 1.07 \text{ bits/ OCDMA chip.}$$

When the average number of photons is increased to $\mu = 80$ photons per 16-ary level, the performance results for an OCDMA transmission with Poisson shot noise are shown in Fig. 17. The achieved spectral efficiency at BER $= 10^{-9}$ improves to

$$\eta = 418 \times \left(\frac{1}{2} \times 2 \times \frac{239}{255}\right) \times P_{ch} \times \frac{62}{64} = 1.21 \text{ bits/OCDMA chip.}$$

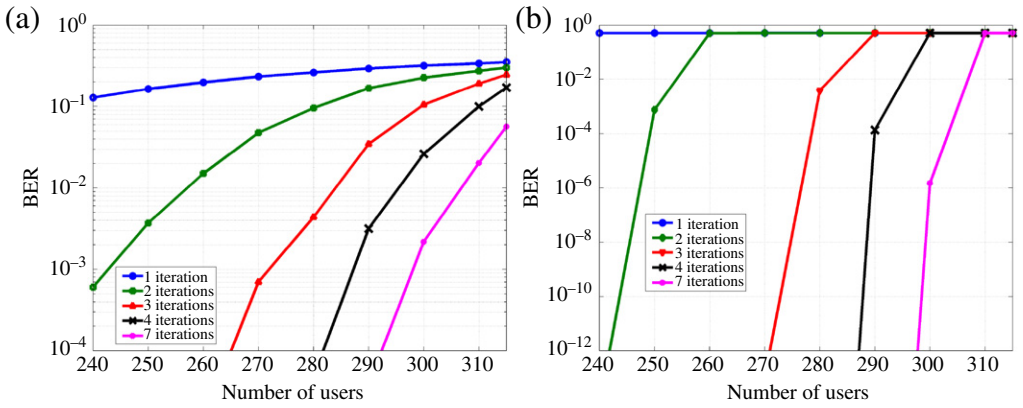

Fig. 15. (Color online) BER performance of the designed 16-ary OCDMA transmission corrupted by Poisson shot noise, when the number of photons per 16-ary level is $\mu = 20$: (a) after convolutional decoding and (b) after both convolutional and Reed–Solomon decoding.

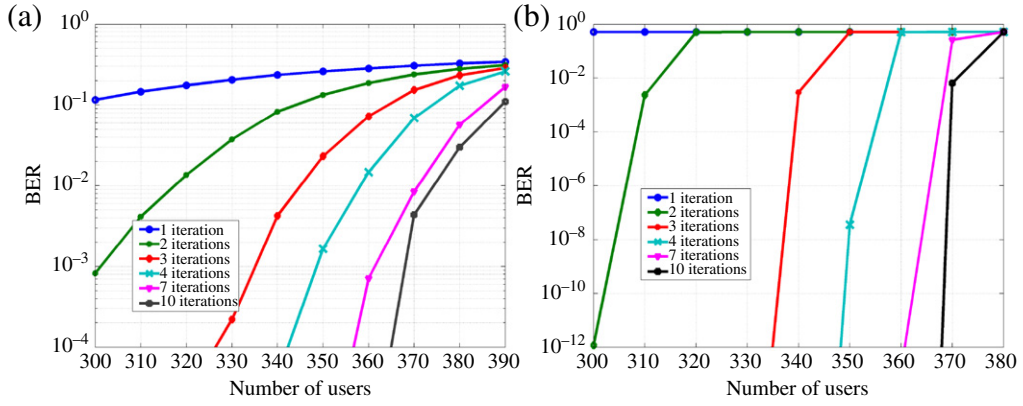

Fig. 16. (Color online) BER performance for the designed 16-ary OCDMA transmission scheme with non-uniform signaling in the presence of Poisson shot noise. The number of photons per 16-ary level is $\mu = 40$ and the BER is shown after (a) convolutional decoding and (b) both convolutional and Reed–Solomon decoding.

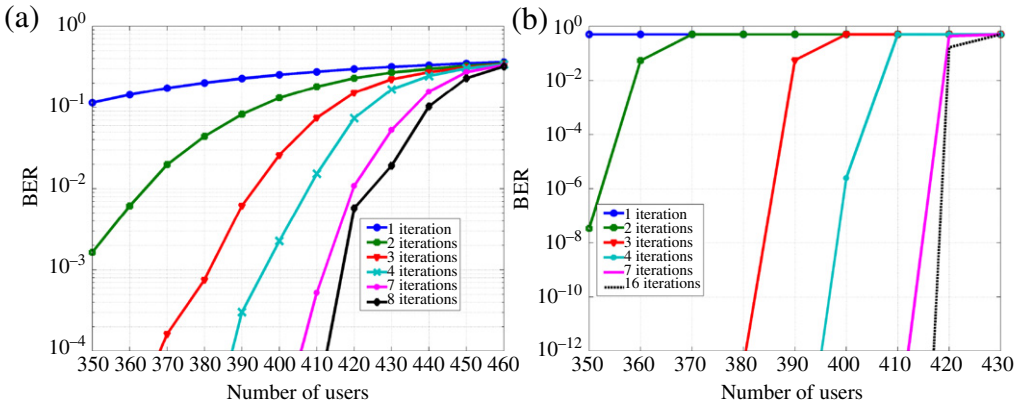

Fig. 17. (Color online) BER results of the designed 16-ary OCDMA transmission scheme with non-uniform signaling when shot noise with $\mu = 80$ photons per 16-ary level corrupts the transmission after (a) convolutional decoding and (b) both convolutional and Reed–Solomon decoding.

Moreover, we also considered the OCDMA network transmission with thermal noise from the receiver electronics, modeled by an AWGN noise. (The normalized chip-level channel SNR is defined as $1/\sigma^2 = 20$ dB.) The simulation results in Fig. 18 demonstrate that the proposed OCDMA scheme can support an even larger number of active users. Indeed, after 12 decoding iterations, up to $K = 462$ active users can be supported at the target BER $= 10^{-9}$. The achieved spectral efficiency is

$$\eta = 462 \times \left(\frac{1}{2} \times 2 \times \frac{239}{255}\right) \times \frac{62}{64} \times P_{ch} = 1.34 \text{ bits/OCDMA chip}.$$

C. Observations and Discussion

Overall, the designed coded M-ary OCDMA system from Fig. 12 performs well in all cases considered in Subsection V.B. We observed that a significant BER performance improvement occurs as the iterative receiver iterates and eliminates the effects of MUI and channel noise from the soft decisions provided by the OCDMA demodulator. The achieved spectral efficiency and BER performance results show that the proposed M-ary OCDMA transmission scheme is robust to several impairments encountered in OCDMA transmission, i.e., MUI, Poisson-distributed shot noise and Gaussian-distributed thermal noise.

In addition, we also observe that as the average number of photons per symbol level increases, the performance of the proposed M-ary OCDMA system with Poisson shot noise improves. Hence, in the limiting case of high average number of transmitted photons, the system performance is not much limited by the Poisson noise, but the MUI becomes the main source of errors.

It is interesting to note that the considered *non-uniform* M-ary OCDMA transmission scheme achieved a spectral efficiency of 1.34 bits per chip, which is significantly better than what the best *uniform* M-ary OCDMA system can achieve (0.72 bits per chip based on the capacity analysis results in Section III). Furthermore, the spectral efficiency of 1.34 bits per chip, achieved by the considered non-uniform M-ary OCDMA transmission with AWGN thermal noise, is

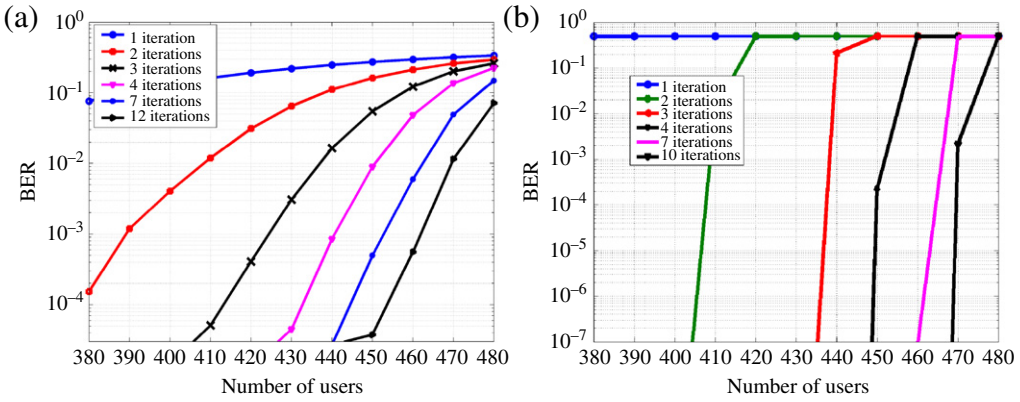

Fig. 18. (Color online) BER of the proposed 16-ary OCDMA transmission system with AWGN thermal noise and non-uniform input signaling after (a) iterative decoding and (b) iterative decoding followed by RS decoding.

- almost twice the spectral efficiency of 0.74 bits/chip achieved by the best previous binary OCDMA system [15];
- more than three times better than the 0.36 bits/chip achieved by the M-ary OCDMA system reported in [14].

Finally, it is interesting to observe that the key reason behind the achieved high OCDMA spectral efficiency is the reduction of the number of actively interfering users K_t. To illustrate this point in further detail, Fig. 19(a) shows the number of actively interfering users K_t on the channel for $K = 300$ active OCDMA network users and channel access probability $P_{ch} = 0.0032$. It can be seen that although the total number of active network users $K = 300$ is high, K_t is rather small. This observation is also illustrated in Fig. 19(b) through the probability distribution of K_t for a large number of active users K. Therefore the single-user receiver has to deal with significantly reduced MUI due to the transmitters' actions (i.e., appropriate non-uniform M-ary signaling). This MUI reduction in turn allows benefit to be gained from the rate increase due to M-ary signaling, when compared to binary or uniform M-ary OCDMA.

VI. Conclusion

This paper presented capacity results and insights for M-ary OCDMA network transmission in the presence of MUI, Poisson shot noise and AWGN thermal noise. It was observed that the use of appropriate non-uniform M-ary signaling leads to reduction of the MUI and high achievable spectral efficiencies. Using the insights from the capacity results, we presented the design of a time/wavelength M-ary OCDMA network transmission scheme that relies on single-user demodulation/decoding and error-control coding.

The simulated BER performance results illustrated that the designed M-ary OCDMA scheme allows the achievement of high spectral efficiencies of up to 1.34 bits per OCDMA chip and can support large numbers of active users. Furthermore, the proposed scheme is robust against several impairments which occur in OCDMA network transmission such as MUI, Poisson shot noise and AWGN thermal noise. Finally, insights were presented which explain the improved performance achieved by the designed M-ary OCDMA system.

Appendix A

This appendix discusses how the OCDMA network receivers from Fig. 12 can tune into the transmission of a particular transmitting user when dealing with network broadcasting and/or multicasting. The appendix also describes how the receiver can determine the value of K_t that is used for soft-decision demodulation in Section IV. Finally, it also presents the probability distribution of the reduced MUI for the proposed OCDMA transmission that uses non-uniform M-ary signaling.

Appendix A.1 Networking Considerations

One way to achieve the objectives described in the previous paragraph is by dedicating two additional wavelengths for OCDMA network protocol implementation.

The wavelength $(\Lambda + 1)$ would be used to determine K_t, the number of actively interfering users who transmitted data (not zero-padded symbols) at time instant t. In particular, when at time t a user transmits T coded symbols over Λ wavelengths of the optical channel he/she also sends a unit intensity signal at the dedicated wavelength $(\Lambda+1)$. (Note that the user sends a zero intensity signal at this wavelength when sending padded zero-padded symbols at time t.) As a result, the combined optical signal intensity at wavelength $(\Lambda + 1)$ at time t is proportional to K_t, the number of users sending non-zero-padded symbols at this time instant.

The wavelength $(\Lambda + 2)$ can be used to allow frame synchronization and tuning into transmission of a particular user by a receiver or receivers in the case of broadcasting/multicasting. In particular, each user uses a user-specific optical time-spreading sequence to distinguish his/her transmitter from other transmitters. When the user is actively sending data over the network using wavelengths $\lambda = 1, 2, 3, \ldots, \Lambda$, his/her optical time-spreading sequence is also transmitted periodically at

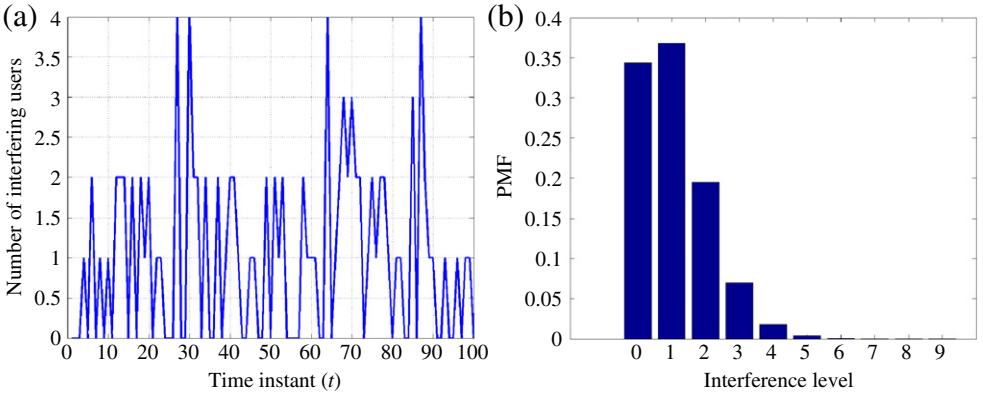

Fig. 19. (Color online) The number of actively interfering users K_t when the total number of users is $K = 300$ for the proposed OCDMA scheme, when $M = 16$ and the channel access probability is $P_{ch} = 0.0032$: (a) K_t is shown at different time instants t; (b) histogram of K_t.

wavelength $(\Lambda+2)$. Although this optical-spreading sequence is not used for actual data transmission at wavelength $(\Lambda+2)$, a receiver or receivers can use a traditional OCDMA matched filter to scan the wavelength $(\Lambda+2)$ for the presence of the desired user. Occurrence of the autocorrelation peak in the matched filter output indicates that the desired user is active and the peak's timing can be used to adjust/synchronize the receiver to the frame timing of the particular transmitter. Finally, the pseudo-random interleavers, used by the OCDMA transmitters in Fig. 12, can be fixed for each user and specified by seed in a common pseudo-random number generator, so that all receivers know the interleavers parameters.

Appendix A.2 Reduced Multi-user Interference

It is also interesting to observe that the proposed OCDMA transmission approach reduces the amount of MUI even when a large number of *active users* K is transmitting data over the OCDMA network. Indeed, the probability mass function of the number of *actively interfering users* K_t is given, for $0 \le j \le K-1$, by

$$P(K_t = j) = \binom{K-1}{j} (1-P_{ch})^{K-1-j} (P_{ch})^{j}. \tag{15}$$

For a large number of users, the above probability reduces to

$$P(K_t = j) \longrightarrow \frac{1}{j!}\left(\frac{M}{M-1}\right)^{j} e^{-\frac{M}{M-1}},$$

which corresponds to a Poisson distribution with parameter $M/(M-1)$. Note that $P(K_t = j)$ is quickly decreasing for $j \ge 1$, as illustrated in Fig. 19. Consequently, the number of interfering users K_t is usually low at each time instant t, even when the total number of active network users K is very large. As an example, for the $M = 16$ modulation level and $K = 500$ active users on the network, the probability of having five or less actively interfering users is 0.9971.

ACKNOWLEDGMENTS

This work was supported in part by the National Science and Engineering Research Council (Canada) and the Canadian Foundation for Innovation. This work has been presented, in part, at IEEE Globecom 2007.

REFERENCES

[1] P. R. Prucnal, *Optical Code Division Multiple Access: Fundamentals and Applications*. CRC Press, 2006.

[2] G. C. Yang and W. C. Kwong, *Prime Codes With Applications to CDMA Optical and Wireless Networks*. Artech House, 2002.

[3] L. Tančevski and I. Andonovic, "Wavelength hopping/time spreading code division multiple access systems," *Electron. Lett.*, vol. 30, pp. 1388–1390, 1994.

[4] M. R. Dale and R. M. Gagliardi, "Channel coding for asynchronous fiber optic CDMA communications," *IEEE Trans. Commun.*, vol. 43, pp. 2485–2492, 1995.

[5] K.-I. Kitayama, "Code division multiplexing lightwave networks based upon optical code conversion," *IEEE J. Sel. Areas Commun.*, vol. 16, pp. 1309–1319, 1998.

[6] H. M. H. Shalaby, "Chip-level detection in optical code division multiple access," *J. Lightwave Technol.*, vol. 16, pp. 1077–1087, 1998.

[7] H. M. H. Shalaby, "Complexities, error probabilities, and capacities of optical OOK-CDMA communication systems," *IEEE Trans. Commun.*, vol. 50, pp. 2009–2017, 2002.

[8] E. Inaty, H. Shalaby, P. Fortier, and L. A. Rusch, "Multirate optical fast frequency hopping CDMA system using power control," *J. Lightwave Technol.*, vol. 20, pp. 166–176, 2002.

[9] P. Azni, M. Nasiri-Kenari, and J. A. Salehi, "Soft-input decoder for decoding of internally channel coded fiber-optic CDMA communication systems," *IEEE Trans. Commun.*, vol. 50, pp. 1994–2002, 2002.

[10] R. M. H. Yim, J. Bajcsy, and L. R. Chen, "A new family of 2-D wavelength-time codes for optical CDMA with differential detection," *IEEE Photonics Technol. Lett.*, vol. 15, pp. 165–167, 2003.

[11] A. J. Mendez, R. M. Gagliardi, V. J. Hernandez, C. V. Bennett, and W. J. Lennon, "Design and performance analysis of wavelength/time (W/T) matrix codes for optical CDMA," *J. Lightwave Technol.*, vol. 21, pp. 2524–2533, 2003.

[12] C.-S. Bres, I. Glesk, R. J. Runser, T. Banwell, P. R. Prucnal, and W. C. Kwong, "Novel M-ary architecture for optical CDMA using pulse position modulation," in *Proc. of the 18th Annu. Meeting of the IEEE Lasers and Electro-Optics Society*, 2005, pp. 982–983.

[13] T. Miyazawa and I. Sasase, "Enhancement of tolerance to MAIs by the synergistic effect between M-ary PAM and the chip-level receiver for optical CDMA systems," *J. Lightwave Technol.*, vol. 24, pp. 658–666, 2006.

[14] A. A. Garba, R. M. H. Yim, J. Bajcsy, and L. R. Chen, "Analysis of optical CDMA signal transmission: capacity limits and simulation results," Special Issue on Optical Information Processing, *EURASIP J. Appl. Signal Process.*, vol. 2005, pp. 1603–1616.

[15] A. A. Garba and J. Bajcsy, "A new approach to achieve high spectral efficiency in wavelength-time OCDMA network transmission," *IEEE Photonics Technol. Lett.*, vol. 19, pp. 131–133, 2007.

[16] C. Berrou, A. Glavieux, and P. Thitimajshima, "Near Shannon limit error-correcting coding and decoding: turbo-codes," in *Proc. of the IEEE Int. Conf. Communications*, 1993, pp. 1064–1070.

[17] S. B. Wicker and V. K. Bhargava, Eds., *Reed-Solomon Codes and Their Applications*. IEEE Press, 1994.

[18] G. Ungerboeck, "Channel coding with multilevel/phase signals," *IEEE Trans. Inf. Theory*, vol. 28, pp. 55–67, 1982.

[19] L. Bahl, J. Cocke, F. Jelinek, and J. Raviv, "Optimal decoding of linear codes for minimizing symbol error rate," *IEEE Trans. Inf. Theory*, vol. 20, pp. 284–287, 1974.